An indication of spin-transition accompanied by an order-disorder structural transformation in [Ni(phpyNO)$_2$(NCS)$_2$] (phpyNO = *tert*-butyl 5-phenyl-2-pyridyl nitroxide)†

Yukiya Kyoden and Takayuki Ishida [iD] *

Reaction of nickel(II) thiocyanate and *tert*-butyl 5-phenyl-2-pyridyl nitroxide (phpyNO) afforded a 2p–3d–2p heterospin triad [Ni(phpyNO)$_2$(NCS)$_2$]. The compound crystallizes in the orthorhombic *Pbcn* space group. The whole molecule is crystallographically independent. The torsion angles around Ni–O–N–C$_{2py}$ are 26.8(4) and 27.3(4)° at 400 K, indicating appreciable orbital overlaps of the radical π* and nickel(II) 3d$_{x^2-y^2}$/3d$_{z^2}$ orbitals. In a low-temperature region, the torsion was enhanced, and the space group changed to monoclinic *P*2$_1$/*c* with a doubled asymmetric unit volume. The χ$_m$*T* value was practically null below *ca.* 140 K and, on heating to 400 K, gradually increased and reached 1.30 cm^3 K mol^{-1}. A van't Hoff analysis suggests a spin transition at *T*$_{1/2}$ = 530(20) K. Density functional theory calculation reproduced ground *S*$_{total}$ = 0 with singlet–triplet gaps of 910 and 1263 K for the 140 K structure, and the gap was reduced to 297 K at 400 K. Consequently, the present compound can be considered as an incomplete spin-crossover material, as a result of *T*$_{1/2}$ located above the experimental temperature window.

Introduction

Persistent organic free radicals are potential building blocks for molecule-based materials showing magnetic, chromic, conducting, and related functions, and they attract much attention from materials chemists.[1,2] The wide diversity of paramagnetic centres and mutual spatial arrangements are available in heterospin systems, in the context of frontier orbital engineering. Gatteschi *et al.* have proposed the versatile "metal–radical approach", where strong magnetic exchange coupling is operative in direct coordination bonds between paramagnetic metal ion and organic radical chromophores.[3]

The exchange coupling in 3d^9-copper(II)- and 3d^8-nickel(II)-radical complexes is the best described in 3d–2p compounds.[3–5] The magnetic (singly-occupied) orbitals are well defined as metal dσ (3d$_{x^2-y^2}$ for copper(II), 3d$_{x^2-y^2}$ and 3d$_{z^2}$ for nickel(II)) and radical π* orbitals. Ferromagnetic coupling occurs when magnetic orbitals are arranged in a σ–π* orthogonal manner. On the other hand, an orbital overlap between them given by breakdown of the orthogonal arrangement (a metal ion lifted above the ligand π-conjugation nodal plane for example) leads to antiferromagnetic interaction.[6] The exchange interaction is

sensitive to the coordination geometry, and the magnitude sometimes exceeds a thermal energy of 300 K, whether ferro- or antiferromagnetic.

Among spin-crossover (SCO) materials, switching between *S* = 0 and *S* = 2 states is the most popularly examined in 3d^6 iron(II) complexes.[7,8] When SCO occurs between dia- and paramagnetic states, concomitant alteration of physical properties would be dramatic. A number of ligands having a *tert*-butyl nitroxide (aminoxyl) group have been developed for building blocks in 2p–3d heterospin[5,9] as well as 2p–4f heterospin[10] compounds. There have been only two examples reported at present on the spin transition between *S*$_{total}$ = 0 ⇄ 2,[11,12] where two *S* = 1/2 paramagnetic ligands and an *S* = 1 nickel(II) centre are involved. What "spin crossover" covers may be extended to multi-centred systems showing an essentially similar spin-multiplicity switch at their ground state.[11–13] The spin state is regulated by ferro-/antiferromagnetic balance continuum in multi-centred systems,[11] in place of the Hund/aufbau principles, or potential/kinetic exchange interactions, in one-centred systems.

According to the mechanism of entropy-driven SCO, a high-spin state is low-lying in a high-temperature phase because of an enhanced entropy term in *G* = *H* − *TS*. Entropy as a temperature coefficient becomes larger when a higher spin multiplicity is realized. The critical temperature *T*$_c$ is defined where the level crossing of the energies of high-spin (HS) and low-spin (LS) states takes place, as depicted in Fig. 1. As for

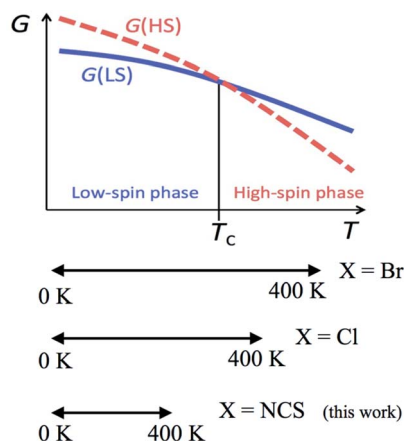*Department of Engineering Science, The University of Electro-Communications, Chofu, Tokyo 182-8585, Japan. E-mail: takayuki.ishida@uec.ac.jp*
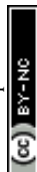
Fig. 1 A schematic Gibbs energy diagram for spin–transition materials. The experimental temperature windows of [Ni(phpyNO)$_2$X$_2$] are also shown in a lower panel.

copper(II)- and nickel(II)-radical chelates, the experiments revealed non-planar chelate rings found in the LS phase while highly planar chelate rings in the HS phase. This scenario has been established for [Ni(phpyNO)$_2$X$_2$] with X = Cl[11] and Br[12] (phpyNO = *tert*-butyl 5-phenyl-2-pyridyl nitroxide;[6a] Fig. 2). The purpose of this paper is to describe what happens in the X = NCS case.

Results

Molecular design and preparation

The previous reports on [Ni(phpyNO)$_2$X$_2$] with X = Cl,[11] Br[12] gave a hint to a molecular design using pseudohalogen coligands. A steric effect may modulate SCO phenomenon. Complex [Ni(phpyNO)$_2$(NCS)$_2$] was facilely prepared by mixing solutions of the paramagnetic ligand and commercially available Ni(NCS)$_2$ in an established manner.[11,12] The complex was characterized by means of IR spectroscopic, elemental, and X-ray crystallographic analyses, clarifying the absence of solvent molecules.

Structural study

Single-crystal X-ray diffraction on [Ni(phpyNO)$_2$(NCS)$_2$] was performed at several temperatures, and the molecular structures at 140 and 400 K are shown in Fig. 3 and 4, respectively. Selected crystallographic data and geometrical parameters are summarized in Tables 1 and 2, respectively. The crystal consists of discrete molecules. A heterospin triad 2p–3d–2p was
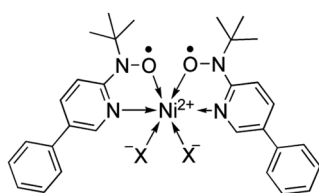

Fig. 2 Structural formula of [Ni(phpyNO)$_2$X$_2$].

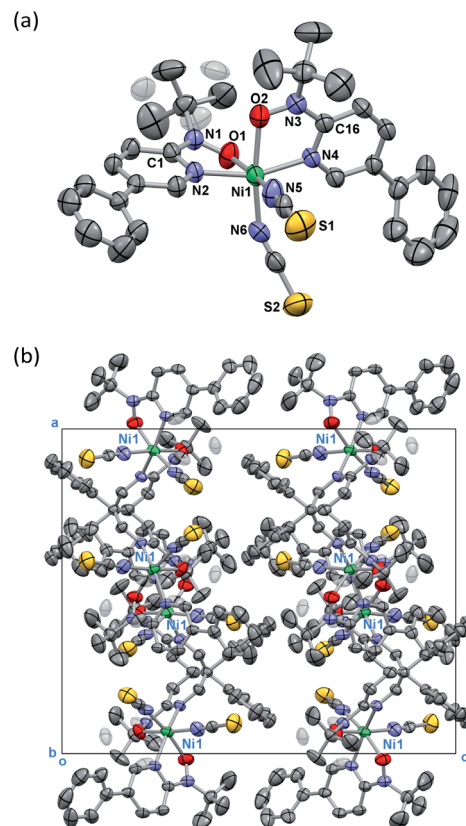**Fig. 3** (a) Crystal structure of [Ni(phpyNO)$_2$(NCS)$_2$] measured at 400 K. Disordered methyl groups (0.39(2) occupancy) are shaded. (b) Molecular packing in a unit cell. Hydrogen atoms are omitted for the sake of clarity. Thermal ellipsoids are drawn at the 30% probability level.

constructed, with five-membered chelate rings involving a direct nickel-nitroxide bond. The coligand NCS$^-$ is coordinated at a nitrogen atom. The coordination geometry of the nickel(II) ion is approximately octahedral, indicating $S_{Ni2+} = 1$. No meaningful residual electron density due to solvent molecules was found. Interestingly, the variable temperature analysis clarified that the present compound underwent an order–disorder structural transition. The transition occurred in a single-crystal-to-single-crystal manner, but the residual R factors were relatively unsatisfactory, owing to deterioration of the single crystal on varying temperature.

The compound crystallizes in an orthorhombic *Pbcn* space group. A whole molecule corresponds to a crystallographically independent unit. A disorder was observed in a *tert*-butyl group, and the occupancy factor was refined to be 0.61(2)/0.39(2) at 400 K (Fig. 3a). According to the magneto-structure relationship,[6,12] the torsion angle M–O–N–C$_{2py}$ ϕ is a convenient index to evaluate the atomic displacement from the ligand π-conjugation plane. In the present compound, the torsion angles around Ni–O–N–C$_{2py}$ are 26.8(4) and 27.3(4)° at 400 K, indicating appreciable orbital overlaps of the magnetic radical and nickel orbitals. A non-bonded O1···O2 distance is relatively short (2.867(5) Å) but slightly longer than the sum of the van der Waals radii (2.8 Å for O/O).[14]
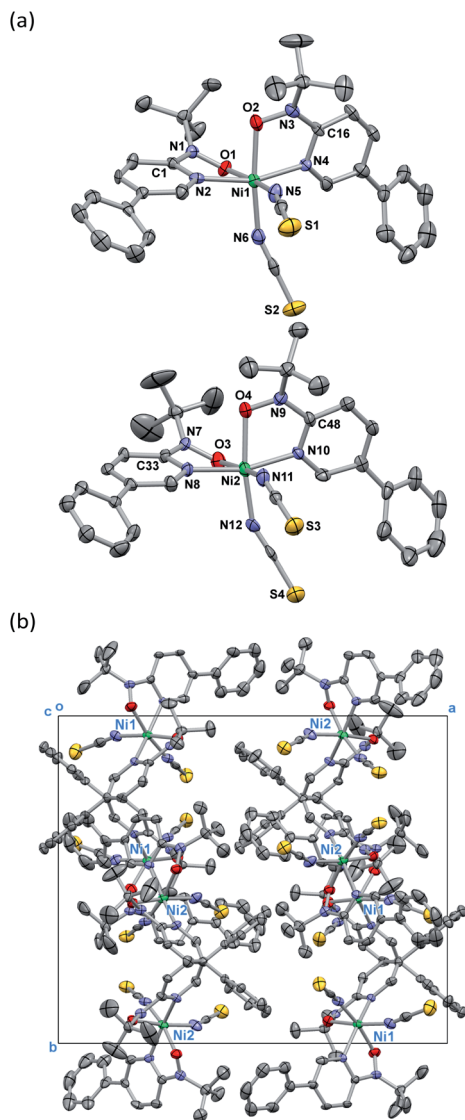
(a)

(b)

Fig. 4 (a) Crystal structure of [Ni(phpyNO)$_2$(NCS)$_2$] measured at 140 K. Two crystallographically independent molecules are shown. (b) Molecular packing in a unit cell. Hydrogen atoms are omitted for the sake of clarity. Thermal ellipsoids are drawn at the 50% probability level.

Table 1 Selected crystallographic parameters of [Ni(phpyNO)$_2$(NCS)$_2$] at 140 and 400 K

Formula	C$_{32}$H$_{34}$N$_6$NiO$_2$S$_2$	
Formula weight	657.48	
T/K	140	400
Crystal system	Monoclinic	Orthorhombic
Space group	$P2_1/c$	$Pbca$
a/Å	19.990(4)	17.0732(19)
b/Å	16.865(3)	19.194(3)
c/Å	18.965(3)	20.667(3)
β/deg	90.338(10)	90
V/Å^3	6394(2)	6772.7(16)
Z	8	8
d_{calcd}/g cm^{-3}	1.366	1.290
μ(MoKα)/mm^{-1}	0.777	0.733
Number of total reflections	11 745	7078
$R(F)$ ($I > 2\sigma(I)$)^a, $wR(F^2)$ (all refls)^b	0.0997, 0.2298	0.0698, 0.1563
Goodness-of-fit parameter	1.038	1.015

^{a} $R = \Sigma[|F_o| - |F_c|]/\Sigma|F_o|$. ^{b} $wR = [\Sigma w(F_o^2 - F_c^2)/\Sigma wF_o^4]^{1/2}$.

Table 2 Bond lengths (Å), bond angles (°), and torsion angles (°) for [Ni(phpyNO)$_2$(NCS)$_2$] at 140 and 400 K

T/K	140	400^a
Ni1–O1, Ni2–O3	2.053(6), 2.049(6)	2.043(3)
Ni1–O2, Ni2–O4	2.046(6), 2.052(6)	2.066(3)
Ni1–N2, Ni2–N8	2.042(7), 2.034(7)	2.059(3)
Ni1–N4, Ni2–N10	2.039(6), 2.039(7)	2.049(3)
Ni1–N5, Ni2–N11	2.012(8), 2.019(9)	1.997(4)
Ni1–N6, Ni2–N12	2.030(8), 2.020(8)	2.030(4)
O1–N1, O3–N7	1.278(8), 1.312(8)	1.287(4)
O2–N3, O4–N9	1.309(8), 1.302(8)	1.292(4)
O1···N2, O3···N4	2.872(8), 2.847(8)	2.867(5)
O1–Ni1–N2, O3–Ni2–N8	75.2(3), 76.5(3)	75.90(13)
O2–Ni1–N4, O4–Ni2–N10	77.1(2), 75.5(3)	75.56(14)
O1–Ni1–N5, O3–Ni2–N11	171.9(3), 171.8(3)	171.77(15)
O2–Ni1–N6, O4–Ni2–N12	171.2(3), 169.0(3)	170.56(14)
Ni1–O1–N1–C1, Ni2–O3–N7–C33	−33.7(8), −38.2(8)	−26.8(4)
Ni1–O2–N3–C16, Ni2–O4–N9–C48	35.8(8), 38.2(7)	27.3(4)

^{a} The Ni2 molecule is identical to the Ni1 molecule.

350, and 400 K were solved in an orthorhombic unit cell while those at 140 and 200 K in a monoclinic cell. The torsion angle monotonically increases on cooling. The oxygen atoms are

On the other hand, the disordered *tert*-butyl portion became ordered at 140 K. Namely, the molecule is differentiated into two independent molecules, called Ni1 and Ni2 molecules, each of which has an ordered *tert*-butyl conformation (Fig. 4a). The symmetry elements were reduced, giving a monoclinic unit cell with $\beta = 90.338(10)°$. The space group changed to $P2_1/c$. It is a normal trend that the low-temperature phase has a lower symmetry.[15,16] The chelate plane is further deformed, as indicated with the Ni–O–N–C$_{2py}$ torsion angles of 33.7(8), 35.8(8), 38.2(8), and 38.2(7)° at 140 K. Despite such molecular transformation, the crystal packing motif is practically unchanged across the structural transformation (Fig. 3b and 4b).

Fig. 5 displays the plot of the torsion angles against temperature for [Ni(phpyNO)$_2$(NCS)$_2$], where structures at 300,
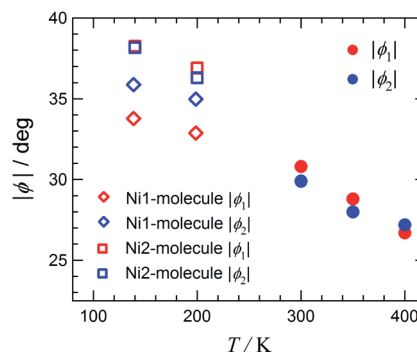

Fig. 5 Torsion angles (|ϕ (Ni–O–N–C$_{2py}$)|) *vs.* temperature plot.

located under the control of the conformational potential surface, regulated by the *tert*-butyl angular positions. As a result, the separation of ϕ's is distinct. In other words, the ordering of *tert*-butyl conformation is proven to be substantial in Fig. 5.

One may wonder whether the determined structure is an identical geometry or an average in time or in space.[17] As Fig. 5 shows, the 400 K structure is a transient structure, as indicated with a considerable slope of ϕ against T at 400 K, but the thermal ellipsoids of the oxygen atoms are normal (Fig. 3). Furthermore, an energy level-crossing could occur between the continuous functions of T (Fig. 1). Therefore, in the present case, every structure has an identical geometry with an identical HS-LS energy gap, but magnetic properties are averaged over contributions from each level having thermal population.

Magnetic study

Magnetic susceptibility of $[Ni(phpyNO)_2(NCS)_2]$ was measured from 1.8 to 400 K at 0.5 T (Fig. 6a). The $\chi_m T$ value was 1.30 cm³ K mol⁻¹ at 400 K, being much smaller than the theoretical spin-only value, 1.75 cm³ K mol⁻¹. A considerable positive slope remained at 400 K. Upon cooling from 400 to 1.8 K, the $\chi_m T$ value approaches null. The presence of strong antiferromagnetic interaction is indicated, and the coupling must be attributed to the intramolecular 2p–3d relations from the structural study. In the low temperature phase the magnetic

(a)

(b)

Fig. 6 (a) The $\chi_m T$ vs. T plot for $[Ni(phpyNO)_2(NCS)_2]$. The solid line is a calculated curve. For the equation and parameters, see the text. (b) van't Hoff plot from the same data. The solid line is drawn with an intercept of 1.409 ($= \Delta S/R$) and a slope of -747 K ($= -\Delta H/R$), where R is the gas constant.

properties are given as an average from those of two independent molecules (see above). The antiferromagnetic couplings totally agree with the prediction from the coordination structure. According to Okazawa's formalism,[18] the critical angle ϕ_c is 21(1)°. All of the ϕ values recorded here fell in the antiferromagnetic region.

As described above, the molecular structure is changed (Fig. 3 and 4), and the exchange interaction is sensitive to the structure. Therefore the van Vleck analysis using constant exchange coupling is inappropriate. Instead, the magnetic data of $[Ni(phpyNO)_2(NCS)_2]$ were assumed to obey the van't Hoff equation (eqn (1)). Such an equilibrium model has often been applied to analyse spin-transition behaviour.[19,20]

$$\gamma_{HS} = \frac{1}{1 + \exp\left[(\Delta H/R)\left(1/T - 1/T_{1/2}\right)\right]} \quad (1)$$

$$\chi_m T = C_0\,\gamma_{HS} + C_1 \quad (2)$$

The experimental $\chi_m T$ value was reduced to the molar fraction of the HS molecules (γ_{HS}) (eqn (2)), where C_0 and C_1 imply the Curie constants for the HS state and the paramagnetic impurity bias, respectively. A satisfactory linear fit appeared in the van't Hoff plot (Fig. 6b) with the parameters optimized, as follows: $C_0 = 3.29(12)$ cm³ K mol⁻¹, $C_1 = 0.0246(7)$ cm³ K mol⁻¹, $T_{1/2} = 530(20)$ K, and the enthalpy change $\Delta H = 6.21(7)$ kJ mol⁻¹. The C_0 value is reasonably acceptable in comparison with the theoretical spin-only $S = 2$ value (3.0 cm³ K mol⁻¹). The very small C_1 indicates the high purity of the sample. The relatively large statistic error of $T_{1/2}$ is unavoidable from the fitting analysis on the onset data. The entropy change was estimated as $\Delta S = 12(1)$ J K⁻¹ mol⁻¹ from the relation $T_{1/2} \Delta S = \Delta H$, because ΔG vanishes at equilibrium. In short, the present compound exhibited thermally induced spin transition, but the thermal energy is insufficient even at 400 K. The domain model[20] indicates an almost uncooperative system from the very gradual spin-transition profile.

Symmetry-breaking transition,[15] order-disorder transition in particular,[16] often has connection with multi-step and/or hysteretic SCO. It seems to be a rare case;[21] though the space group and crystal system have been changed, the SCO profile keeps one-step and nonhysteretic.

DFT calculation study

To check the exchange coupling change depending on the structure, the density functional theory (DFT) calculation[22] was performed to the determined structure of $[Ni(phpyNO)_2(NCS)_2]$. The self-consistent field (SCF) energies on the 140 and 400 K structures were calculated on the UB3LYP/6-311+G(2d,p) level. At 140 K (Fig. 7a), the lowest state was singlet, drawn as ↓-↑↑-↓ for the spin structure in N1O1–Ni–O2N3. The highest one was quintet, ↑-↑↑-↑. Two triplet states, ↑-↑↑-↓ and ↓-↑↑-↑, intervene them. The energy gaps between the ground and the first excited states are 910 and 1263 K for the Ni1 and Ni2 molecules, respectively, which are much larger than the thermal energy of a conventional experimental temperature range.
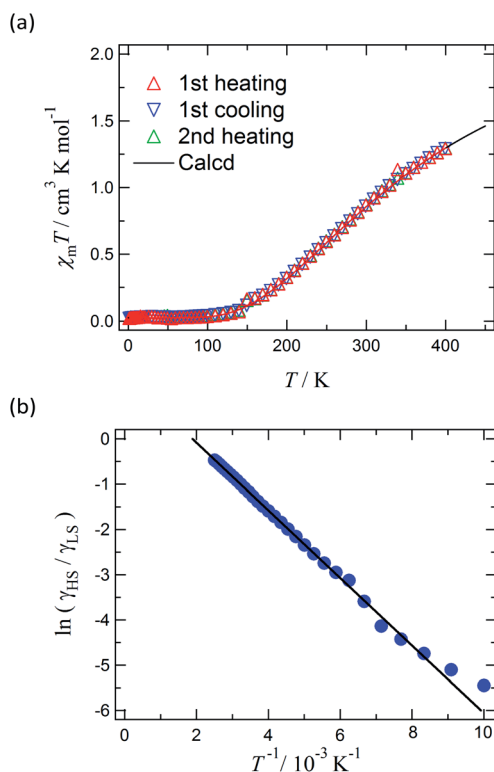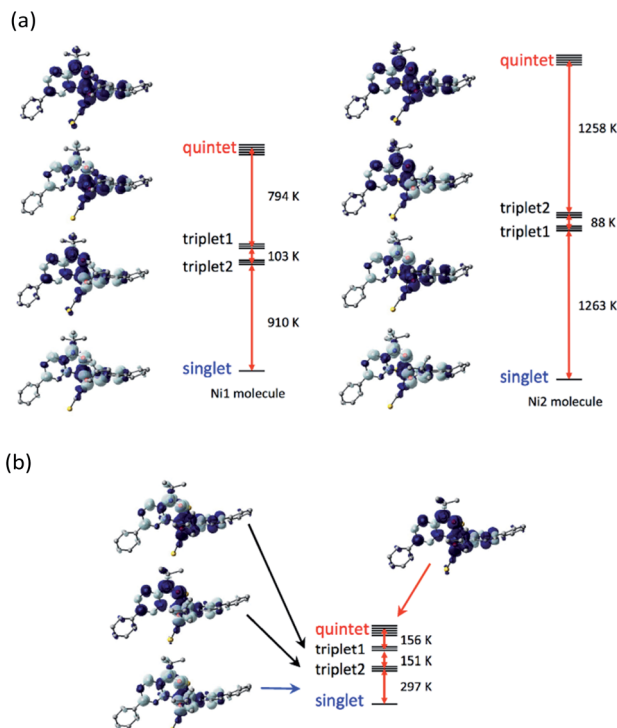
(a)

(b)

Fig. 7 Diagram of the relative energy levels of the singlet, two triplet, and quartet states for (a) the 140 K form (Ni1 and Ni2 molecules) and (b) the 400 K form of $[Ni(phpyNO)_2(NCS)_2]$. The geometries were given from the crystallography. Dark and light lobes imply the positive and negative spin densities, respectively, with an isocontour of 0.002 e$^-$ Å^{-3}.

The ground state remained singlet at 400 K (Fig. 7b), indicating that the exchange couplings are both antiferromagnetic in the entire temperature range here. However, we have to pay attention to the fact that the energy gap between the ground and the first excited states became as narrow as 297 K, which is comparable to the temperatures where the magnetic properties were measured.

Quantification of the exchange coupling parameter J in the spin Hamiltonian $H = -2J(S_1 \cdot S_2 + S_2 \cdot S_3)$ does not give high reliability solely from this calculation. The problem resides in the accidentally short intramolecular radical–radical distance.[12]

Discussion

Now let us overview the results on the derivatives with X = Cl,[11] Br,[12] and NCS (this study). The $T_{1/2}$ order is as follows: $T_{1/2}(Br) < T_{1/2}(Cl) < T_{1/2}(NCS)$ (Table 3). This situation is illustrated in the bottom of Fig. 1. The present compound can be considered as an incomplete spin-crossover (or pseudo spin-transition[23]) material, as a result of $T_{1/2}$ located far above the experimental temperature window.

The ligand field splitting is not important in the present SCO scenario, because the HS/LS states are regulated by 3d–2p ferro-/antiferromagnetic exchange interactions. The crystallographic analysis clarified that the coligands occupied the trans positions of the radical oxygen atoms. The *trans*-influence order is known to be Cl$^-$ < Br$^-$ < NCS$^-$,[24] suggesting that the stronger

Table 3 Bond lengths (Å), torsion angles (°), and thermodynamic parameters for $[Ni(phpyNO)_2X_2]$ at 400 K

Coligand X	Cl	Br	NCS
Ni1–O1	2.083(3)	2.060(4)	2.043(3)
Ni1–O2	2.103(3)	2.094(4)	2.066(3)
Ni1–O1–N1–C1	13.0(4)	10.4(7)	26.8(4)
Ni1–O2–N3–C16	25.8(3)	25.9(6)	27.3(4)
$T_{1/2}$/K	173.7(8)	134(1)	530(20)
ΔH/kJ mol^{-1}	4.57(5)	3.22(6)	6.21(7)
ΔS/J K^{-1} mol^{-1}	26.3(1)	24.0(7)	12(1)
References	11	12	This work

ligand would bring about the weaker trans bond. As summarized in Table 3, unexpectedly, the shortest Ni–O bond lengths were characterized in the NCS derivative. The bond strength is supposed to have relation to a covalent character due to the strong 3d–2p antiferromagnetic coupling.

Steric effects from the coligands seem to be key, because the order of the van der Waals radii and covalent radii is $r(N) < r(Cl) < r(Br)$,[14] which coincides with the $T_{1/2}$ order. The following is one of possible explanations. Sterically bulky coligands suppress out-of-plane distortion of the chelate rings, while smaller coligands can accommodate atomic displacement out of the chelate plane in a nickel(II) coordination sphere. Thus, bulkiness stabilizes the HS state and causes a low-temperature shift of $T_{1/2}$.

The entropy change of SCO can be interpreted as a sum of electronic, vibrational, and conformational terms. The electronic contribution is given with the degeneracy of each state.[25] In the case where singlet and quintet states are involved, the electronic contribution is given as $\Delta S_{elec} = R \ln\{(2S_{HS} + 1)/(2S_{LS} + 1)\} = R \ln 5 = 13.38$ J K^{-1} mol^{-1}. We have to assume the conformational contribution $\Delta S_{conf} = R \ln 2 = 5.76$ J K^{-1} mol^{-1} from the order-disorder structural transition. In addition, vibrational contribution ΔS_{vib} is present as well in total ΔS. The previous works on the $[Ni(phpyNO)_2X_2]$ reported reasonable $\Delta S = 26.3(1)$ and 24.0(7) J K^{-1} mol^{-1} for X = Cl[11] and Br,[12] respectively. It should be noted that comparably small $\Delta S = 12(2)$ J K^{-1} mol^{-1} was obtained here.

However, the small ΔS does not necessarily imply the lower spin multiplicity at the high-temperature phase. The following notices strongly suggest that the ground state should be HS in the high-temperature phase: (1) the driving force is required for structural modification toward a planar chelate on both wings when heated. (2) Order–disorder-type structural transition is often accompanied by spin transition. (3) The Curie constant of the high-temperature phase is $C_0 = 3.29(12)$ cm^3 K mol^{-1}, being quite compatible with theoretical one for the quintet species. It is inevitable that the ground state is depopulated under high-temperature conditions, and effective ΔS from the experimental data may be short accordingly.

Conclusions

The present compound, doubly chelated $[Ni(phpyNO)_2(NCS)_2]$, has been synthesized as a 2p–3d–2p heterospin triad. The

exchange coupling is strongly antiferromagnetic in a low-temperature structure whilst moderately antiferromagnetic in a high-temperature structure. The $T_{1/2}$ value is estimated to be 530(20) K. This compound can be considered as an incomplete spin-crossover material because the molecular structure at 400 K still is an intermediate toward the HS structure. Even if temperature is raised sufficiently above $T_{1/2}$, the susceptibility could not reach the theoretical HS value owing to a thermal depopulation effect.

We have to stress that the exchange parameter J is a function of temperature. Detailed structural study is needed to reveal a gradual structural transformation. In comparison among the Cl, Br, and NCS derivatives, the order is shown as $T_{1/2}(Br) < T_{1/2}(Cl) < T_{1/2}(NCS)$. The unconventional scenario of the multi-centred spin crossover seems to be plausible after the col-igand dependence on $T_{1/2}$ is overviewed.

Experimental section

Preparation and characterization

After combining a dichloromethane solution (0.65 mL) containing phpyNO[6a] (72.5 mg; 0.301 mmol) and a methanol solution (0.90 mL) containing $Ni(NCS)_2$ (26.8 mg; 0.153 mmol) at room temperature, the mixture was allowed to stand a few h. Dark red needles of $[Ni(phpyNO)_2(NCS)_2]$ were precipitated, collected on a filter, and air-dried. The yield was 24.9 mg (0.0378 mmol; 25%). Mp. 191 °C (dec.). IR (attenuated total reflection (ATR)) 2983, 2061, 1450, 1256, 1176, 1011, 760, 689, 554 cm^{-1}. Anal. Calcd. for $C_{32}H_{34}N_6NiO_2S_2$: C, 58.46; H, 5.21; N, 12.78; S, 9.75%. Found: C, 58.20; H, 5.52; N, 12.82; S, 9.62%. A polymorphic non-SCO byproduct was obtained as hexagonal-shaped dark red plates in another run. IR (ATR): 2988, 2092, 2071, 1451, 1258, 1178, 1010, 764, 697, 555 cm^{-1}. Anal. Calcd. for $C_{32}H_{34}N_6NiO_2S_2$: C, 58.46; H, 5.21; N, 12.78; S, 9.75%. Found: C, 58.19; H, 5.35; N, 12.78; S, 9.50%. This byproduct crystallized in a monoclinic $P2/c$ space group with $a = 17.843(4)$, $b = 11.274(3)$, $c = 17.612(5)$ Å, $\beta = 112.001(11)°$.

Crystallographic analysis

X-Ray diffraction data of a single crystal of $[Ni(phpyNO)_2(NCS)_2]$ were acquired on a Rigaku Saturn70 diffractometer with a CCD detector and graphite monochromated Mo Kα radiation ($\lambda = 0.71073$ Å). The structures were solved in the CRYSTAL-STRUCTURE program,[26] and the parameters were refined in the Shelxl program.[27] Selected crystal data are summarized in Table 1, and important geometrical parameters are listed in Table 2.

Magnetic analysis

Magnetic susceptibilities of polycrystalline $[Ni(phpyNO)_2(NCS)_2]$ were acquired on a Quantum Design MPMS XL-7 SQUID magnetometer. The magnetic response was corrected with diamagnetic blank from the sample holder measured separately. The diamagnetism of the sample itself was estimated from Pascal's constant.

DFT calculation

Density functional theory (DFT) calculations were performed with the Gaussian03 rev. C.02.[22] A single-point calculation was applied to the geometry of $[Ni(phpyNO)_2(NCS)_2]$ from the X-ray crystallography. The self-consistent field energy was converged to 10^{-7} a.u. on the UB3LYP[28]/6-311+G(2d,p) level. The broken symmetry method[29] was utilized.

Conflicts of interest

There are no conflicts to declare.

Acknowledgements

Notes and references

1 (*a*) *Stable Radicals: Fundamentals and Applied Aspects of Odd-Electron Compounds*, ed. R. G. Hicks, Wiley, Chichester, UK, 2010; (*b*) H. Iwamura, *Polyhedron*, 2013, **66**, 3; (*c*) I. Ratera and J. Veciana, *Chem. Soc. Rev.*, 2012, **41**, 303; (*d*) *Nitroxides. Brief History, Fundamentals, and Recent Developments*, ed. G. I. Likhtenshtein, Springer, Switzerland, 2020.

2 (*a*) B. K. Rugg, B. T. Phelan, N. E. Horwitz, R. M. Young, M. D. Krzyaniak, M. A. Ratner and M. R. Wasielewski, *J. Am. Chem. Soc.*, 2017, **139**, 15660; (*b*) X. Ai, Y. Chen, Y. Feng and F. Li, *Angew. Chem., Int. Ed.*, 2018, **57**, 2869; (*c*) K.-A. Hansen and J. P. Blinco, *Polym. Chem.*, 2018, **9**, 1479.

3 (*a*) A. Caneschi, D. Gatteschi, R. Sessoli and P. Rey, *Acc. Chem. Res.*, 1989, **22**, 392–398; (*b*) X. Meng, W. Shi and P. Cheng, *Coord. Chem. Rev.*, 2019, **378**, 134.

4 (*a*) D. Luneau, P. Rey, J. Laugir, P. Fries, A. Caneschi, D. Gatteschi and R. Sessoli, *J. Am. Chem. Soc.*, 1991, **113**, 1245; (*b*) A. Ali, D. Dhar, S. K. Barman, F. Lloret and R. Mukherjee, *Inorg. Chem.*, 2016, **55**, 5759; (*c*) M. S. de Souza, M. Briganti, S. G. Reis, D. Stinghen, C. S. Bortolot, R. A. Cassaro, G. P. Guedes, F. C. da Silva, V. F. Ferreira, M. A. Novak, S. Soriano, F. Totti and M. G. F. Vaz, *Inorg. Chem.*, 2019, **58**, 1976.

5 (*a*) A. Okazawa, T. Nogami and T. Ishida, *Chem. Mater.*, 2007, **19**, 2733; (*b*) K. Osanai, A. Okazawa, T. Nogami and T. Ishida, *J. Am. Chem. Soc.*, 2006, **128**, 14008; (*c*) C. Aoki, T. Ishida and T. Nogami, *Inorg. Chem.*, 2003, **42**, 7616.

6 (*a*) A. Okazawa, Y. Nagaichi, T. Nogami and T. Ishida, *Inorg. Chem.*, 2008, **47**, 8859; (*b*) A. Okazawa, T. Nogami and T. Ishida, *Polyhedron*, 2009, **28**, 1917.

7 M. A. Halcrow, *Spin-Crossover Materials: Properties and Applications*, John Wiley & Sons, Ltd., Oxford, UK, 2013.

8 (*a*) G. Aromí and J. A. Real, Special Issue "Spin Crossover (SCO) Research", *Magnetochemistry*, 2016, **2**, 28; (*b*) K. Takahashi, Special Issue "Spin-Crossover Complexes", *Inorganics*, 2018, **6**, 32; (*c*) T. Kitazawa, Special Issue "Synthesis and Applications of New Spin Crossover

Compounds", *Crystals*, 2019, **9**, 382; (*d*) S. Hayami, S. M. Holmes and M. A. Halcrow, Themed Issue "Spin-State Switches in Molecular Materials Chemistry", *J. Mater. Chem. C*, 2015, **3**, 7767.

9 (*a*) A. Okazawa, D. Hashizume and T. Ishida, *J. Am. Chem. Soc.*, 2010, **132**, 11516; (*b*) A. Okazawa and T. Ishida, *Inorg. Chem.*, 2010, **49**, 10144.

10 (*a*) T. Kanetomo, T. Kihara, A. Miyake, A. Matsuo, M. Tokunaga, K. Kindo, H. Nojiri and T. Ishida, *Inorg. Chem.*, 2017, **56**, 3310; (*b*) T. Kanetomo, T. Yoshitake and T. Ishida, *Inorg. Chem.*, 2016, **55**, 8140; (*c*) T. Ishida, R. Murakami, T. Kanetomo and H. Nojiri, *Polyhedron*, 2013, **66**, 183–187.

11 Y. Homma and T. Ishida, *Chem. Mater.*, 2018, **30**, 1835.

12 Y. Kyoden, Y. Homma and T. Ishida, *Inorg. Chem.*, 2019, **58**, 10743.

13 V. Ovcharenko, S. Fokin, E. Chubakova, G. Romanenko, A. Bogomyakov, Z. Dobrokhotova, N. Lukzen, V. Morozov, M. Petrova, M. Petrova, E. Zueva, I. Rozentsvelg, E. Rudyakova, G. Levkovskaya and R. Sagdeev, *Inorg. Chem.*, 2016, **55**, 5853.

14 (*a*) A. Bondi, *J. Phys. Chem.*, 1964, **68**, 441; (*b*) P. Pyykko and M. Atsumi, *Chem. – Eur. J.*, 2009, **15**, 186.

15 N. Ortega-Villar, M. C. Munoz and J. A. Real, *Magnetochemistry*, 2016, **2**, 16.

16 (*a*) M. Griffin, S. Shakespeare, H. J. Shepherd, C. J. Harding, J. –F. Létard, C. Desplanches, A. E. Goeta, J. A. K. Howard, A. K. Powell, V. Mereacre, Y. Garcia, A. D. Naik, H. Muller-Bunz and G. G. Morgan, *Angew. Chem., Int. Ed.*, 2011, **50**, 896; (*b*) C. F. Sheu, S. Pillet, Y. C. Lin, S. M. Chen, I. J. Hsu, C. Lecomte and Y. Wang, *Inorg. Chem.*, 2008, **47**, 10866.

17 R. Sanchez-de-Armas, N. C. Hernandez and C. J. Calzado, *Inorg. Chem. Front.*, 2019, **6**, 1228.

18 A. Okazawa, *IOP Conf. Ser.: Mater. Sci. Eng.*, 2017, **202**, 012002.

19 O. Kahn, *Molecular Magnetism*, VCH, New York, 1993, ch. 4.

20 R. Boca, *Theoretical Foundations of Molecular Magnetism: Current Methods in Inorganic Chemistry*, Elsevier, Amsterdam, 1999, vol. 1.

21 A. Kashiro, K. Some, Y. Kobayashi and T. Ishida, *Inorg. Chem.*, 2019, **58**, 7672.

22 M. J. Frisch, *et al.*, *Gaussian 03 revision C.02*, Gaussian Inc., Wallingford, USA, 2004.

23 F. Lanfranc de Panthou, E. Belorizky, R. Calemczuk, D. Luneau, C. Marcenat, E. Ressouche, P. Turek and P. Rey, *J. Am. Chem. Soc.*, 1995, **117**, 11247.

24 (*a*) T. G. Appleton, H. C. Clark and L. E. Manzer, *Coord. Chem. Rev.*, 1973, **10**, 335; (*b*) D. F. Shriver and P. W. Atkins, *Inorganic Chemistry*, Oxford Univ. Press, Oxford, 4th edn., 1999, ch. 20.

25 (*a*) G. Molnar, M. Mikolasek, K. Ridier, A. Fahs, W. Nicolazzi and A. Bousseksou, *Ann. Phys.*, 2019, **531**, 1900076; (*b*) J. Cirera, M. Via-Nadal and E. Ruiz, *Inorg. Chem.*, 2018, **57**, 14097; (*c*) M. Valtiner, H. Paulsen, P. Weinberger and W. Linert, *MATCH*, 2007, **57**, 749.

26 *CRYSTALSTRUCTURE, version 4.2*, Rigaku/MSC, The Woodlands, TX, 2010–2015.

27 G. M. Sheldrick, SHELXL-2016/6, *Acta Crystallogr., Sect. C: Struct. Chem.*, 2015, **71**, 3.

28 (*a*) A. D. Becke, *J. Chem. Phys.*, 1993, **98**, 5648; (*b*) C. Lee, W. Yang and R. G. Parr, *Phys. Rev. B*, 1988, **37**, 785.

29 K. Yamaguchi, Y. Takahara and T. Fueno, in *Applied Quantum Chemistry*, ed J. V. H. Smith, H. F. Schaefer and K. Morokuma, Reidel, Dordrecht, 1986, pp. 155–184.